Geospatial Governance for Sustainable Water Resources Management: Integrating SWAT Modeling, Satellite Data, and Hydrogeological Units in Padsan River Watershed

Jimenez, J. I.,[1,2,3*] Tripathi, N. K.,[2] Pandey, A.,[4] Shrestha, S.,[5] Chao, K. C.,[6] Gatela Jr., E. Q.,[7] Jimenez Jr., J. I.,[8] and Aspiras, J. E.[9]

[1]Department of Water Resources Development and Management, Indian Institute of Technology-Roorkee, Roorkee, India 247667

[2]Remote Sensing and Geographic Information Systems, Asian Institute of Technology, Pathum Thani, 12120, Thailand, E-mail: julius_ij@wr.iitr.ac.in,* https://orcid.org/0009-0001-4036-8024, E-mail: nitinkt@ait.ac.th, https://orcid.org/0000-0001-5618-2841

[3]Mariano Marcos State University, City of Batac (2906), Ilocos Norte, Philippines

[4]Department of Water Resources Development and Management, Indian Institute of Technology-Roorkee, Roorkee, India 247667, E-mail: ashish.pandey@wr.iitr.ac.in, https://orcid.org/0000-0003-2110-8283

[5]Water Engineering and Management, Asian Institute of Technology, Pathum Thani 12120, E-mail: sangam@ait.ac.th, https://orcid.org/0000-0002-4972-3969

[6]Geotechnical Engineering, Asian Institute of Technology, Pathum Thani, Thailand 12120 E-mail: geoffchao@ait.asia, https://orcid.org/0000-0001-5473-4526

[7]Environmental Engineering Management, Asian Institute of Technology, Pathum Thani, Thailand 12120, E-mail: st124238@ait.ac.th

[8]Philippine Rice Research Institute – Batac, City of Batac (2906), Ilocos Norte, Philippines

[9]GeoSpatial Science and Technology Hub (GeoSpada Hub), Ilocos Norte, Philippines, E-mail: judithaspiras318@gmail.com

**Corresponding Author*

DOI: https://doi.org/10.52939/ijg.v21i10.4525

Abstract

Groundwater governance in the Philippines is challenged by limited irrigation infrastructure, reliance on aquifers, and increasing climate variability. This study presents a geospatial governance framework for sustainable water management in the Padsan River Watershed (PRW), located in Northern Luzon. The framework integrates the Soil and Water Assessment Tool (SWAT), bias-corrected satellite climate products, hydrogeological unit mapping, and high-resolution estimates using building-footprint-based population mapping derived from Google building footprints. The integration approach has yielded an efficient hydrological model that effectively captures the occurrence of the water balance. The model simulation results show pronounced seasonality in river discharge, significant variation in groundwater recharge across Land Use/Land Cover (LULC), and spatial mismatches between irrigation service areas and productive aquifers. Population overlays reveal that the majority of residents rely on highly productive but potentially stressed groundwater systems, while several potential irrigation zones remain underserved. These findings underscore the importance of aligning water supply infrastructure with both hydrological potential and demand while ensuring resource sustainability. The study concludes with recommendations, including the extension of infrastructure, the implementation of Managed Aquifer Recharge (MAR) systems, and the creation of a centralized GIS-based decision support system for equitable and climate-resilient water planning. By combining satellite data, modeling, and demographic analytics, the proposed framework provides a replicable approach to strengthen water governance in data-scarce river basins.

Keywords: CHIRPS, Conjunctive Use Management, ERA5 Land, Groundwater Governance, Satellite-derived Products, SWAT

1. Introduction

Groundwater is the planet's most extensive and reliable source of freshwater, significantly contributing to global drinking water supplies and sustaining critical sectors such as agriculture, industry, and ecosystem services [1] and [2]. However, this essential resource is facing growing pressures from population growth, rapid urbanization, changing land-use patterns, and the intensifying impacts of climate change [3] and [4]. In numerous developing countries, including the Philippines, these pressures are exacerbated by institutional fragmentation, insufficient data integration, and inadequate policy frameworks [5] and [6]. As groundwater recharge becomes increasingly unpredictable and demand continues to escalate, there exists an urgent necessity for spatially explicit and community-informed governance strategies to ensure long-term water security.

The Padsan River Watershed (PRW), situated in the Ilocos Region of Northern Luzon, illustrates a compelling case for the advancement of integrated approaches. This watershed fulfills multiple water demands, encompassing irrigation for rice and corn production, as well as urban and rural domestic water supply, along with the expansion of peri-urban settlements [7]. Agricultural intensification and population growth have exerted considerable pressure on the region's water resources. At the same time, climatic extremes, such as prolonged droughts associated with El Niño phenomena, have intensified risks to groundwater recharge and sustainability [8] and [9]. Further complicating these challenges is the limited capacity of local institutions to access and operationalize scientific data for policymaking, particularly in relation to the subsurface water environment.

Addressing these governance and development challenges necessitates the integration of geospatial tools, hydrological modeling, and demographic analytics within a participatory and inclusive framework. The utilization of the Soil and Water Assessment Tool (SWAT), a physically-based and spatially distributed hydrological model, provides valuable insights into the dynamics of surface-groundwater interactions under varying land use/land cover (LULC) and climate scenarios [10] and [11]. Prior studies in the Philippines have demonstrated the effectiveness of SWAT in modeling surface and subsurface flow across diverse watershed settings [12][13] and [14]. Furthermore, the application of high-resolution population distribution estimates presents an innovative method for identifying potential water stress zones, particularly in regions where census data may be outdated or unavailable [15]. In this study, *"high-resolution population distribution estimates"* refers to a fine-scale population estimate generated through a building-footprint-based population allocation method, where official census counts are redistributed into individual building footprints from the Google Open Buildings dataset (sub-30 m resolution) [16].

This study introduces the novelty of integrating SWAT-based hydrological modeling with satellite-derived climate inputs, fine-resolution population distribution estimates from Google's building footprints [16] and hydrogeological mapping. Unlike conventional census-based approaches that provide only village or municipal-level aggregates and global gridded (100 m) population estimate alternatives, the building-footprint method disaggregates population to a resolution of 10 to 30 m, unveiling settlement patterns and demand hotspots that are often missed in coarse datasets. Globally, techniques akin to "mapping the world population one building at a time" demonstrate that satellite-derived building datasets combined with census totals can yield high-resolution population maps at approximately 30 m scale. Building on earlier Philippine SWAT studies that focused on surface water flow in hydropower [12][17][18] and [19] and surface water [20][21] and [22], this work explicitly integrates surface-groundwater interaction with fine-scale population demand and aquifer characteristics. Moreover, the integration of institutional-sourced hydrogeological data with geospatial analysis enhances the understanding of aquifer systems and recharge potential within the watershed. By combining these analyses with population estimates, this methodology facilitates the spatial linkage between water availability and human demand. This approach significantly strengthens the evidence base for identifying critical zones, potential areas for managed aquifer recharge, equitable resource distribution, and adaptive water governance [23].

In pursuit of supporting sustainable water governance and enhancing community resilience in the Padsan River Watershed, this study aims to quantify and model groundwater processes, thereby generating actionable insights that bolster community participation, institutional coordination, and policy reform in the water sector. The emphasis on lifelong learning for sustainable development resonates strongly with the study's intent to democratize access to hydrological information and promote adaptive decision-making at both local and regional levels. Specifically, the study aims to (1) simulate and analyze the spatiotemporal patterns of groundwater recharge utilizing the SWAT model with satellite-based derived products (SDPs);

(2) employ Google's building footprint data to estimate spatial population distribution, enabling the identification of high-demand areas; (3) map and evaluate hydrogeological units to inform sustainable abstraction practices and Managed Aquifer Recharge interventions; and (4) formulate evidence-based recommendations for equitable water resource allocations, integrated watershed management, and climate-resilient urban and agricultural planning.

Through this integrated geospatial and hydrological approach, the study contributes to a transdisciplinary understanding of groundwater governance, aligning science with action to support impact-driven development and empowered communities.

2. Methodology

2.1 Study Area

The Padsan River Watershed (PRW, Figure 1), also known as the Laoag River Basin, is the largest in the province of Ilocos Norte, Philippines, covering approximately 1,320 km² (Figure 1). Originating from the Cordillera Mountains, the river traverses the province's central and western regions, including the capital, Laoag City, before discharging into the West Philippine Sea. It plays a vital role in supporting agriculture and urban development in the province. Its riparian zones and coastal dunes provide essential ecosystem services, including food sources, storm protection, habitats for diverse flora and fauna, and maintenance of water quality [24]. The watershed experiences a Type 1 climate, as classified by the Philippine Atmospheric, Geophysical and Astronomical Services Administration (PAGASA) using the Modified Coronas Classification (MCC) [25]. MCC categorizes regions based on the seasonality of average monthly rainfall [26], with less than 100 mm classified as dry, while a wet month exceeds this threshold. Out of 4 types, Type 1 climate is characterized by a distinct dry season from November to April and a wet season from May to October [25]. Rainfall is highly seasonal, with peak precipitation occurring in western Luzon, resulting in marked variability in water availability that strongly influences agricultural cycles, river discharge, and groundwater recharge. Climate variability and extreme weather events have heightened hydrological risks [27], including altered river discharge patterns and potential groundwater depletion, threatening water security and agricultural productivity [28]. These challenges necessitate a robust, data-driven, and integrated approach to provide foundational insights for comprehensive management in the face of increasing climate variability.

2.2 Research Methods and Approach

This study adopts an integrative and interdisciplinary methodology framework (Figure 2) that combines hydrological (numerical) modeling, remote sensing, and geospatial analysis to inform sustainable water resource management.

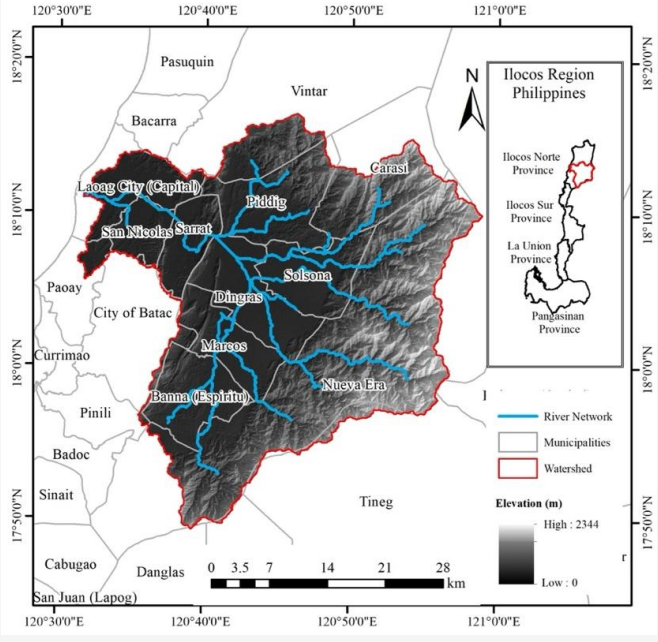

Figure 1: Padsan River Watershed (PRW)

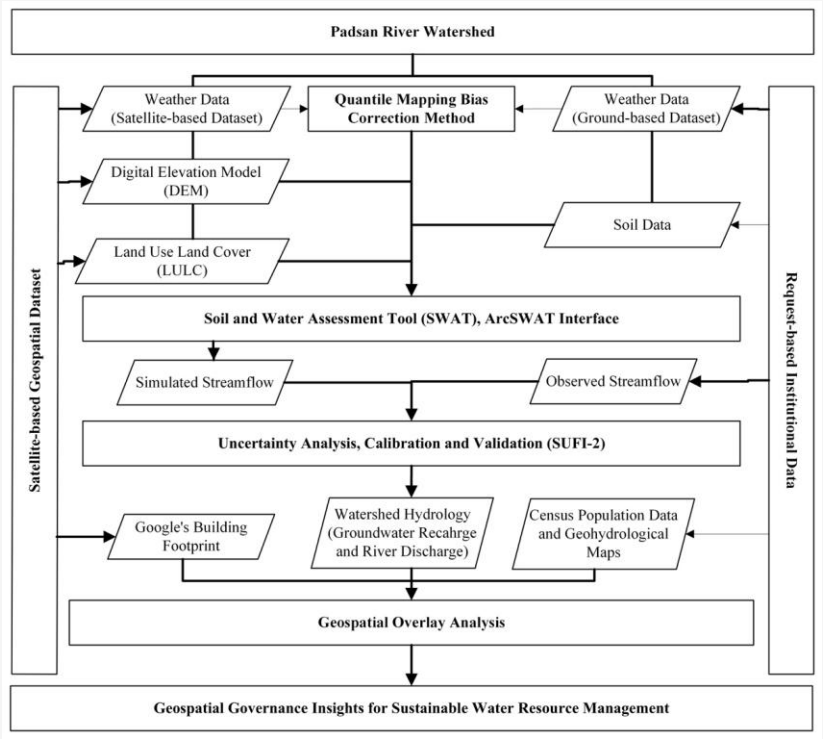

Figure 2: Geospatial governance for sustainable water resources management conceptual framework

Satellite-based geospatial datasets include Climate Hazards Group Infrared Precipitation with Stations (CHIRPS) precipitation, European Centre for Medium-Range Weather Forecasts (ECMWF) Reanalysis v5 Land Dataset (ERA5 Land) temperature, Shuttle Radar Topographic Mission (SRTM) Digital Elevation Model (DEM), Copernicus Land Use/Land Cover (LULC), and Google's building footprints. Request-based institutional data include ground-based station weather data, soil map, streamflow data, hydrogeological unit maps, and census population data.

Satellite climate data (CHIRPS and ERA5 Land) were bias corrected using Quantile Mapping to align with ground observations. The corrected inputs, together with DEM, LULC, and soil data, were processed and used as model input for the Soil and Water Assessment Tool (SWAT) via ArcSWAT to simulate the watershed hydrology. Model calibration and validation were performed using observed streamflow in SWAT-CUP with Sequential Uncertainty Fitting version 2 (SUFI-2), ensuring reliable hydrological outputs. Population distribution was derived from Google's building footprints allocation of census counts, while hydrogeological maps provided aquifer productivity and recharge potential. These datasets were combined through geospatial overlay analysis to identify recharge zones, irrigation gaps, and demand hotspots.

The framework ultimately translates hydrological modeling and population-hydrogeology integration into governance insights, supporting equitable and climate-resilient water resource management in the Padsan River Watershed.

2.3 Integration of Multi-source Geospatial and Institutional Datasets

This study utilized a combination of satellite-based geospatial datasets and institutional data sources to support SWAT model simulations and governance analysis. Table 1 summarizes the data used in this study, their descriptive attributes, and the sources. To ensure reliability and comparability, all datasets underwent preprocessing, resolution harmonization, and temporal alignment before integration. Daily precipitation (CHIRPS v2.0, 0.05° ~5 km) and mean temperature (ERA5-Land 0.01° ~9 km) were bias-corrected using Quantile Mapping (QM) against PAGASA ground-based weather observations. To address spatial mismatches, ERA5-Land was resampled to 0.05° using bilinear interpolation, aligning it with CHIRPS. Temporal coverage was harmonized from 1987 to 2021, the period during which complete overlap across datasets was available. Missing temporal values in ground station data were gap-filled using linear interpolation.

Table 1: Datasets used in the study

Data Input	Data Used	Resolution/Temporal Coverage	Data Source
Elevation Data	SRTM-DEM	30 m (2018)	Earth Explorer (https://earthexplorer.usgs.gov)
Satellite-Based Weather Data – Precipitation	CHIRPS Precipitation	5 km, daily (1987-2021)	Climate Hazards Group Website (https://www.chc.ucsb.edu/data/chirps)
Satellite-Based Weather Data – Temperature	ERA-5 Land Temperature	9 km (1987-2021, daily)	Copernicus Climate Data provider (https://cds.climate.copernicus.eu/cdsapp#!/dataset/reanalysis-era5-land)
LULC	Copernicus LULC	100 m (2021)	Copernicus Land Monitoring Service (https://land.copernicus.eu/en)
Building Footprint	Google's Building Footprint	0.5 m (2021)	Google Open Building Dataset (https://sites.research.google/open-buildings/)
Ground-based Weather data	PAGASA Laoag Station Weather Data	Daily (1987-2021)	PAGASA Climatological Data (https://www.pagasa.dost.gov.ph/climate/climate-data)
Streamflow Data	National Irrigation Administration (NIA) Streamflow Data	Monthly (2003-2021)	NIA – San Nicolas Office
Soil Data	Bureau of Soil and Water Management B(SWM) Soil Map	30 m (2010)	Geoportal Philippines (https://www.geoportal.gov.ph)

Static geospatial inputs, including the Shuttle Radar Topography Mission Digital Model (SRTM-DEM 30 m), Copernicus Land Cover (100 m), soil maps, and hydrogeological units, were projected to WGS84/UTM Zone 51N and clipped to the Watershed, for categorical variables (LULC, soil, hydrogeology, nearest-neighbor resampling preserved class integrity. Building footprint data from Google open Buildings (~0.5 m resolution) [16] and [29] were integrated with census data to generate fine-resolution population distribution estimates. Although global datasets continue to be updated through 2025, this study used data up to December 2021. At the time of analysis (2024-2025), CHIRPS and ERA-5 Land had undergone validation only up to 2021, ensuring complete overlap with PAGASA station data and avoiding preliminary near-real-time records that are subject to revision. The 1987-2021 dataset length (34 years) adequately captures interannual variability and climate extremes for robust hydrological modeling.

2.4 Satellite-based Bias Correction Using the Quantile Method

Satellite-based precipitation and temperature products offer broad spatial coverage and temporal consistency, making them valuable for data-scarce regions like PRW. However, these datasets often exhibit systematic biases due to limitations in satellite retrieval algorithms, spatial resolution differences, and sensor-specific errors [30]. These biases, if uncorrected, can significantly affect hydrological simulations, particularly in models like SWAT that are sensitive to climatic inputs.

Quantile mapping (QM) is a statistical bias correction technique that aligns the empirical cumulative distribution function (CDF) of satellite data with that of observed ground-based data. It corrects not only the mean but also higher-order moments (e.g., skewness), making it more robust than simpler methods, such as linear scaling [30].

To reduce systematic errors in the satellite-based climate datasets, precipitation (CHIRPS) and temperature (ERA-5 Land) were bias-corrected against observed records from the only available PAGASA climate station within the watershed. The correction was performed using the conventional quantile mapping (QM) method [31][32] and [33]. The QM method first computes the empirical cumulative distribution functions (eCDFs) for the observed and satellite datasets. The eCDF is defined in Equation 1:

$$SUIFF(x) = \frac{1}{n}\sum_{i=1}^{n} I(x_i \leq x)$$

Equation 1

Where $F(x)$ is the eCDF, n is the number of data points, x_i represents the data points, and I is the indicator function that is 1 if the condition is actual or 0 otherwise. After computing the empirical CDFs,

the quantile mapping transformation follows the governing equations:

$$x_{corrected} = F_o^{-1}(F_s(x))$$

Equation 2

Where $x_{corrected}$ is the corrected value, F_s is the satellite eCDF, and F_o is the observed eCDF. In practice, Equation 2 ensures that a satellite is mapped to the corresponding quantile in the observed distribution.

The performance of the bias correction was evaluated using different statistical parameters. These are Percent Bias (PBIAS), Root Mean Square Error (RMSE), coefficient of determination (R^2), Mean Absolute Error (MAE), Kling-Gupta Efficiency (KGE), Mean Bias Error (MBE), Standard Deviation Ratio (SDR), and RMSE-Observation Standard Deviation Ratio (RSR). These statistical parameters are computed using Equations 3 to 11:

$$PBIAS = 100\,x\,\frac{\sum(S_i - O_i)}{\sum S_i}$$

Equation 3

$$RMSE = \sqrt{\frac{1}{n}\sum_{i=1}^{n}(S_i - O_i)^2}$$

Equation 4

$$NSE = 1 - \frac{\sum_{i=1}^{n}(O_i - S_i)^2}{\sum_{i=1}^{n}(O_i - \bar{O})^2}$$

Equation 5

$$R^2 = \left[\frac{\sum(O_i - \bar{O})(S_i - \bar{S})}{\sqrt{\sum(O_i - \bar{O})^2 \sum(S_i - \bar{S})^2}}\right]^2$$

Equation 6

$$MAE = \frac{1}{n}\sum_{i=1}^{n}|O_i - S_i|$$

Equation 7

$$KGE = 1 - \sqrt{(r-1)^2 + (\alpha - 1)^2 + (\beta - 1)^2}\ ,\quad \alpha = \frac{\sigma_s}{\sigma_o}\ ,\beta = \frac{\mu_s}{\mu_o}$$

Equation 8

$$MBE = \frac{1}{n}\sum_{i=1}^{n}(S_i - O_i)$$

Equation 9

$$SDR = \frac{\sigma_s}{\sigma_o}$$

Equation 10

$$RSR = \frac{RMSE}{\sigma_o}$$

Equation 11

Where O_i are the observed values at time step i, S_i are the satellite (or corrected satellite or simulated) values at time step i, n is the total number of paired observations or sample size, $\bar{O}$ is the mean of observed values, $\bar{S}$ is the mean of simulated values, α is the variability ratio between the standard deviation of the simulated values (σ_s) and the standard deviation of the observed values (σ_o), β is the bias ratio between the mean of simulated values (μ_s) and the mean of observed values (μ_o), r is the linear correlation coefficient.

PBIAS measures the average tendency of the model to overestimate (negative) or underestimate (positive) predictions, with an ideal value of 0. NSE measures the predictive power of the model relative to the mean observations. Values range from negative infinity to 1, with values greater than 0.5 considered acceptable, and values closer to 1 indicating stronger predictive capabilities. R^2 measures the strength of linear correlation between simulated and observed flows, ranging from 0 to 1, with higher values indicating stronger agreement. RMSE and MAE measure the average magnitude of errors, with RMSU giving greater weight to large deviations; both are ideally 0. KGE is a composite metric that simultaneously measures correlation (r), variability ratio, and bias ratio, and its values range from negative infinity to 1, with 1 representing perfect performance. SDR measures the degree to which simulated variability reflects observed variability, with 1 as the ideal. RSR evaluates the relative size of errors compared to natural variability, with an ideal of 0 and values <0.7 considered satisfactory in hydrological modeling [34]. Together, these metrics evaluate accuracy, correlation, variability, and systematic bias, providing a comprehensive assessment of bias correction. Various parameters are also used in the evaluation of the simulated SWAT model performance.

The QM was applied to monthly data to preserve daily records, which were used as the reference distribution and applied uniformly across all satellite grid cells in the watershed. This ensures internal consistency but assumes that the bias characteristics at the reference station are representative of the watershed.

2.5 SWAT-based Hydrological and Groundwater Recharge Modeling

The Soil and Water Assessment Tool (SWAT) serves as the core model for simulating watershed-scale hydrological processes. The model incorporates topography, soil, LULC, and corrected weather data to generate simulated streamflow at various temporal scales and spatiotemporal patterns of groundwater recharge, which are crucial for identifying recharge zones and supporting Managed Aquifer Recharge (MAR) planning.

The choice of input datasets reflects a balance between accuracy, coverage, and availability in data-scarce watersheds. SRTM DEM (30 m) was selected for reliable watershed delineation at medium scales, while Copernicus Land Cover (100 m) and NAMRIA soil maps provided the best available spatial data for LULC and soil representation. Satellite-based climate datasets CHIRPS precipitation, ERA5 Land temperature were chosen because of their long-term daily records and spatial coverage, which compensate for the limited ground station network; bias correction was anchored on the only PAGASA station within the watershed. Observed discharge data from NIA-San Nicolas Cura RIS Station were used for calibration and validation. These choices, while ensuring reproducibility, introduce limitations such as (a) the relatively coarse resolution of LULC and soil data may underestimate local heterogeneity; (b) reliance on a single ground station for bias correction assumes spatially uniform bias patterns; and(c) calibration at a single station restricts internal spatial validation. Nevertheless, these datasets represent the most consistent, validated, and widely used sources for SWAT applications in data-scarce tropical watersheds.

Model simulation was conducted for the period from 2000 to 2021. A three-year warm-up (2000 to 2002) was applied to minimize initial condition effects. Model calibration was set from 2003 to 2014, while the model validation was from 2015 to 2021. Parameter ranges were selected based on literature values for tropical and monsoon-influenced catchments [35]. These 16 SWAT parameters were referred to in previous work [10], providing guidelines for successful calibration and uncertainty analysis on the SWAT model. The parameter's value ranges are adjusted according to the ranges recommended in [36]. Observed discharge data were obtained from the National Irrigation Administration – San Nicolas Office (NIA-San Nicolas) gauging station at the Cura River Irrigation System (RIS, 18°08′25″N 120°49′53″E). Monthly discharge data were available from 2003 to 2021. Due to data scarcity, calibration and validation relied on this single station, which limits spatial representativeness but provides essential boundary flow information.

Calibration and uncertainty analysis were performed using the SWAT-CUP (SWAT Calibration and Uncertainty Procedures) interface [37]. SWAT-CUP is widely used for calibration, sensitivity analysis, and uncertainty analysis of SWAT models. The SUFI-2 [29] algorithm was employed, which combines sensitivity analysis, calibration, validation, and uncertainty quantification. In SUFI-2, parameter uncertainty is propagated through Latin Hypercube sampling, and results are evaluated using the 95% prediction uncertainty (95 PPU) band. The goal is to maximize the percentage of observed data captured by the 95PPU while minimizing the bandwidth, thus balancing accuracy and uncertainty. Model performance was assessed using standard hydrological statistics. These are R^2 (Equation 6), NSE (Equation 5), Pearson's correlation (r), and RSR (Equation 11).

Calibration was constrained by the availability of one discharge station within PRW, which reduces spatial representativeness and limits calibration of internal watershed dynamics. Nevertheless, using long-term daily to monthly records at the station provided reliable streamflow dynamics for overall water balance assessment.

2.6 Population Distribution and Demand Estimation

Population distribution was estimated by integrating the Google Open Buildings dataset (vector polygons at ~0.5 m resolution) with official census data from the Philippines Statistical Authority (PSA) and widely used by the Provincial Government of Ilocos Norte [7]. The PSA 2020 average household rate (occupancy rate) in each municipality (S_c) was used to represent the building-level population (P_i), as presented in Equation 12:

$$S_c = P_i \quad \text{Equation 12}$$

The method assumes that (a) each building footprint corresponds to a single residential unit, and (b) the PSA-reported average household size, widely used by the government unit [7] applies uniformly to all buildings in a municipality. This method and its assumptions were used, given its comprehensive simplicity and its applicability to the watershed that is dominated by rural and peri-urban areas, where single buildings are highly represented by one household. This, however, has its limitations, as informal or small dwellings not captured in Open Buildings may lead to underestimation. At the same time, inclusion of non-residential structures (e.g.,

schools, warehouses) may cause overestimation. The current method used applies to general purposes (e.g., watershed demand estimation) and may require additional filtration of the building footprint if the technique's purpose requires higher estimation efficiency (e.g., barangay demand estimation). Despite these limitations, this building-footprint-based allocation provides fine-resolution, spatially explicit estimates of population distribution. It improves upon coarse census-based methods and supports the integration of demographic demand with hydrological and hydrogeological analyses in data-scarce watersheds.

Subsequently, to integrate population estimates with hydrogeological zones (and other zones, e.g., LULC), a zonal summation approach (P_k) was computed using Equation 13:

$$P_k = \sum_{i=1}^{n} 1i \in A_k P_i,$$

Equation 13

Where A_k denotes the set of polygons belonging to zonal class k and l_i is an indicator function equal to 1 if building i falls within A_k, and zero otherwise. This ensured that all buildings were uniquely assigned to one aquifer class. In cases where building footprints overlapped multiple zones, centroids were used as the assignment criterion. These will facilitate the identification of high-demand zones for water use and urban-rural population density gradients, thereby assisting in the demand-responsive allocation of water.

2.7 Hydrogeological Unit Mapping and Potential Aquifer Stress

Hydrogeological information for the Padsan River Watershed was derived from the Hydrogeological map of the province of Ilocos Norte (1:250,000) [38] produced under the National Geohazard, Groundwater Assessment, and Responsible Mining Program [39] by the Department of Environment and Natural Resources (DENR). This map was georeferenced and digitized into a GIS database, projected to WGS84/UTM Zone 51N, and clipped to the watershed boundary for analysis. The digitization process ensured that aquifer boundaries, lithological descriptions, and productivity classifications were spatially consistent with other geospatial datasets used in the study.

Hydrogeological units in the Mines and Geoscience Bureau (MGB) map are classified by aquifer productivity based on lithology and well yield criteria established by MGB. Following DENR (2023), aquifers were grouped into four classes: (1) high productivity aquifers (unconsolidated alluvium and volcanic deposits, typically yielding >50 L/s); (2) moderate productivity aquifers (weathered sedimentary formations with yields of 10–50 L/s); (3) low productivity aquifers (consolidated igneous and metamorphic rocks, <10 L/s); and (4) poor/non-aquifers (dense, unfractured rocks with negligible groundwater potential). The classification used in this study, therefore, directly reflects the official hydrogeological criteria validated and established by MGB–DENR [38].

For integration, the digitized hydrogeological units were overlaid with SWAT-derived groundwater recharge maps using zonal statistics to quantify the average recharge associated with each aquifer class. At the same time, building-footprint-based population estimates were aggregated within each hydrogeological unit to estimate the population dependent on aquifers of varying productivity. This integration enabled the identification of aquifer stress zones, defined as areas where high population pressure coincides with low recharge or low productivity aquifers. The methodology is limited by the reliance on national-scale hydrogeological mapping (1:250,000), which may generalize small-scale heterogeneity, and by the absence of detailed well data for local validation. Nevertheless, the MGB–DENR maps represent the most authoritative and consistent assessment available in the Philippines, and their integration with recharge and population datasets provides a robust first-order analysis of groundwater stress in the Padsan River Watershed.

2.8 Geospatial Synthesis and Governance Insights

Finally, the model's outputs and geospatial layers, which encompass population density, groundwater recharge, and hydrogeological information, are synthesized through a geospatial overlay analysis. This facilitates the formulation of scientific and evidence-based governance recommendations for equitable and climate-resilient water governance, along with strategic inputs for integrated watershed governance and sustainable land-use planning.

The methodological framework highlights the fusion of hydrological modeling, remote sensing, and geospatial analytics to address complex challenges in water resources management. By placing scientific outputs within the context of spatial demand, hydrological suitability, and the governance framework, this study contributes actionable insights towards climate-resilient, inclusive, and data-driven watershed and water resources management planning.

3. Results and Discussions

3.1 Corrected Satellite-based Weather Datasets

The application of QM Bias Correction (QMBC) to satellite-based weather datasets, specifically CHIRPS for precipitation and ERA5 for mean temperature (Tmean), demonstrated considerable improvements in the statistical alignment of remote sensing data with ground-based observations. The analysis compared several statistical parameters before and after correction (Table 2), revealing the extent to which QM can enhance the dataset's reliability for hydrological modeling for water resources management studies.

In the case of the CHIRPS precipitation data, the uncorrected dataset already exhibited strong statistical agreement with ground-based observations, reflected in high NSE and R^2 values (> 0.5), where the slight decrease after correction is negligible, as it remains at a satisfactory level. Despite this, a slight positive bias was present (PBIAS = 1.76%), and the SDR was slightly below 1 (0.88), indicating a minor underrepresentation of observed variability. Following bias correction via QMBC, systematic bias was entirely removed (PBIAS ~ 0), and the SDR was improved to exactly 1.0, signifying an efficient match in variability between corrected and observed precipitation. The KGE increased from 0.86 to 0.93, highlighting an overall improvement in dataset quality.

The only notable drawback was a slight increase in the RMSE from 96.06 mm to 100.29 mm, and the subtle rise of RSR from 0.364 to 0.38, which directly incorporates RMSE by standardizing it against the standard deviation of observed data [34]. This is due to adjustments in extreme values, as a study [40] argued that RMSE is highly sensitive to a small number of extreme events because of its squared error formulation. This is also consistent with a study that RMSE may slightly increase even as the mean conditions improve [41]. Similar findings in the survey conducted in Kenya showed that a slight increase in RMSE was observed, but the overall distribution agreement improved [42], including the MAE, which improved in this study from 55.27 mm to 52.39 mm. RMSE measures the square root of average squared differences, which is sensitive to outliers, while MAE measures the average absolute difference between two datasets. Based on MAE, it has more minor errors on average days, while the extreme adjustment triggers the sensitivity of RMSE [40]. Corrected CHIRPS overall performance efficiently represented the observed dataset, considering all the statistical indicators, despite a few drawbacks.

Regarding the ERA5 mean temperature datasets, the uncorrected values exhibited significant deficiencies. The Nash-Sutcliffe Efficiency (NSE) and R^2 values were both approximately zero (0.015 and 0.01, respectively), indicating a minimal correlation with observed values. The dataset was characterized by a cold bias, as reflected in a Mean Bias Error (MBE) of -1.37°C and a Percent Bias (PBIAS) of -4.97°C. The Root Mean Square Error (RMSE) and Mean Absolute Error (MAE) were moderately elevated at 1.66°C and 1.44°C, respectively, while the Standard Deviation Ratio (SDR) of 0.84 suggested an underestimation of variability. Following the application of Quantile Mapping Bias Correction (QMBC), the corrected ERA5 TMEAN dataset demonstrated substantial improvements across all metrics. The NSE and R^2 values both markedly increased to 0.66, confirming a significantly stronger agreement with the observed data. Bias was effectively mitigated, as evidenced by the near-zero MBE and PBIAS. RMSE and MAE were reduced to 0.97°C and 0.77°C, respectively, whereas the SDR approached unity (0.98), indicating that the corrected dataset now accurately represented the variability in the observations. Furthermore, the Kling-Gupta Efficiency (KGE) improved from 0.76 to 0.83, further validating the enhancement in overall statistical fidelity. These improvements render the ERA5 TMEAN dataset considerably more appropriate for downstream applications such as hydrological modeling and vulnerability assessments. The Quantile Mapping Bias Correction method proved effective in improving both the structural accuracy and reliability of CHIRPS and ERA5 datasets. While ERA5 TMEAN experienced significant improvements due to initially poor alignment, CHIRPS benefited more subtly from refinements in its distributional characteristics. The results affirm that QMBC is a vital preprocessing step for ensuring the integrity of satellite-based datasets in hydrological modeling applications.

3.2 Calibrated and Validated SWAT Model

Out of 16 SWAT parameters [35] considered in the study, four were found to be highly sensitive during the sensitivity analysis. These are the baseflow alpha factor ratio, SCS Runoff Curve Number for Moisture condition II, effective hydraulic conductivity (mm/h), and moisture bulk density (g/cm³, Table 3). According to [43], these parameters are primarily identified as sensitive parameters in various studies conducted on tropical watersheds, such as the PRW, which is supported by a review conducted by [44].

Table 2: Statistical validation results of the QM bias correction method

Statistical Parameters	Uncorrected CHIRPS against Ground-Based Rainfall	Corrected CHIRPS Against Ground-Based Rainfall	Uncorrected Era5 Mean Temperature Against Ground-Based Temperature	Corrected Era5 Mean Temperature Against Ground-Based Temperature
NSE (%)	0.87	0.85	0.02	0.66
PBIAS (%)	1.76	-0.00	-4.97	0.01
R^2	0.87	0.86	0.65	0.66
RMSE, (mm)	96.09	100.29	1.66	0.97
MAE, (mm)	55.27	52.39	1.44	0.77
KGE	0.86	0.927	0.76	0.83
MBE	-0.51	0.00	-1.37	0.00
SDR	0.88	1.00	0.84	0.98
RSR	0.364	0.38	0.99	0.58

Table 3: Sensitive SWAT parameters during the Calibration

Swat Parameters	Description	T-Stat/ *P*-Value	Value Range	Fitted Value
V_ALPHA_BNK.RTE	Baseflow alpha factor ratio	-14.94/0.00	0.00 to 1.00	0.03
R_CN2.MGT	SCS Runoff Curve Number for moisture condition II	-14.10/00	0.00 to 2.00	0.08
R_SOL_K().SOL	Effective hydraulic conductivity (mm/hr)	-5.46/0.00	-0.25 to 0.50	-0.19
R_SOL_BD().SOL	Moist bulk density (g/cm³)	-3.64/0.00	0.00 to 1.00	0.66

This comprehensive review revealed that CN2 was consistently sensitive across all studies conducted across the world, while the other three were among the other 12 most sensitive. Moreover, these four sensitive parameters collectively indicate a hydrograph controlled by rapid storm runoff and slow exchange between the floodplain and bank. In the PRW, steep headwaters and Type 1 monsoon storms elevate CN-driven rapid flow. At the same time, the lower alluvial plain with shallow groundwater supports prolonged bank-storage release, consistent with regional hydrogeological [38] and climatic documentation [25]. These sensitive parameters reflect PRW's steep-to-alluvial geomorphology, Type 1 monsoon climate, which is characterized by storm peaks that set infiltration partitioning over compacted lowland soils. At the same time, recessions are governed by slow bank-storage release from the alluvial floodplain. Furthermore, the dominance of baseflow alpha reflects the strong role of aquifer storage and dry-season groundwater contributions in the watershed. CN2's high sensitivity corresponds to the prevalence of agricultural land with compacted soils and variable slopes that strongly control runoff. Sensitivity of hydraulic conductivity and bulk density aligns with the spatial heterogeneity in soil infiltration potential between uplands and lowland agricultural zones. These parameter sensitivities are thus consistent with the watershed's monsoonal hydrology and geophysical attributes.

Furthermore, the sensitivity of the baseflow alpha factor ratio indicates that groundwater discharge is a significant component of streamflow in the PRW. This implies that accurately simulating recharge rates is critical for modeling baseflow contributions. On the other hand, the sensitivity of hydraulic conductivity and bulk density highlights that soil properties govern infiltration and percolation, which directly determine recharge rates. Spatial variability in these parameters drives differences in recharge across the watershed. This highlights the significant contribution of streamflow-based calibrated and validated models in simulating groundwater recharge in the case of a data-scarce region like the PRW. It could provide significant insights for a comprehensive solution for declining water tables and increasing water scarcity (e.g., managed aquifer recharge).

Consequently, the corrected climate dataset for rainfall and temperature, along with other spatiotemporal data, was used to simulate the SWAT model. The calibration and validation performance (Table 4, Figure 3) demonstrated significant efficiency, enabling the extraction of valuable insights for watershed hydrology. During the calibration period 2003 to 2014, the simulated mean river discharge (3.44 m^3/s) closely matched the observed discharge (3.54 m^3/s), with a standard deviation of 3.07 m^3/s compared to the observed 2.73 m^3/s.

Table 4: Statistical calibration and validation results

Statistical Parameters	Calibration (2003-2014)		Validation (2015-2021)	
	Observed River Discharge	Simulated River Discharge	Observed River Discharge	Simulated River Discharge
Mean (m^3/s)	3.54	3.44	3.56	3.06
Standard Deviation	2.73	3.07	2.41	2.89
PBIAS, %	2.80		14.00	
R^2	0.66		0.71	
NSE	0.57		0.54	
r	0.81		0.84	
RSR	0.66		0.68	

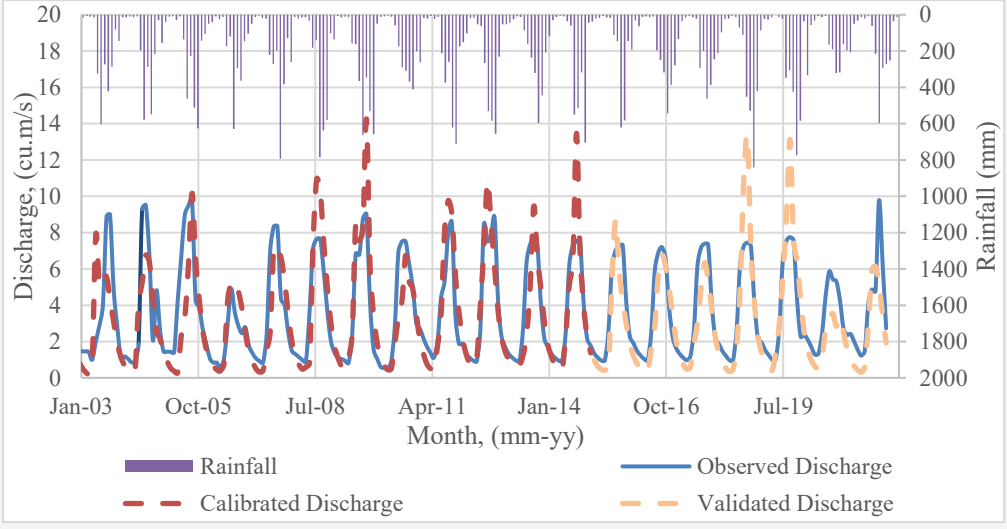

Figure 3: Time series of rainfall and simulated vs. observed streamflow in the Padsan River watershed (2003–2021)

Statistical performance metrics indicated an NSE of 0.56 and an R^2 of 0.66, both reflecting a satisfactory level of agreement between the observed and simulated flow [45]. The Performance Bias (PBIAS) was measured at 2.80, indicating a slight underestimation by the model, which remains well within acceptable limits. Additionally, the RSR value of 0.66 and the Pearson correlation coefficient (r) of 0.81 further substantiated the strong correlation and reasonable predictive power of the model throughout the calibration phase. The validation of the model utilizing an independent dataset spanning from 2015 to 2021 further substantiated the credibility of the model, albeit with a marginal decrease in performance. The observed and simulated mean river discharges were recorded at 3.56 m^3/s and 3.06 m^3/s, respectively, accompanied by a PBIAS of 14%, which denotes a moderate overestimation. This overestimation is attributed to the increasing variability of climate extremes in recent years (validation period) compared to the past years (calibration period). With additional analysis, it is found that the calibration period has higher high extremes (95^{th} percentile = 8.88 m^3/s) and lower low extremes (5^{th} percentile = 0.845 m^3/s) compared to the validation period (95^{th} percentile = 7.44 m^3/s and 5^{th} percentile = 0.96 m^3/s). Furthermore, the ratio between the wet months and the dry months remains approximately 1:1. At the same time, in the validation period, it changes to approximately 3:2. This highlights the increased variability of extreme climate events, which is argued by the findings of [46]. Furthermore, the validation period also coincides with the 2015-2016 El Niño, one of the strongest on record [47], which is reported to have caused widespread drought in the region. During this period, the observed rainfall dataset revealed multiple consecutive dry months, while river discharge significantly dropped to less than 1.8 m^3/s. For these, the study recommends that future work may adopt seasonal calibration and validation (wet and dry seasons) better to capture the constructing hydrological responses of tropical monsoon watersheds and reduce bias during extreme events. Overall, the SWAT model demonstrated reliable performance for reproducing watershed hydrological dynamics, making it suitable for long-term water resources assessment [34].

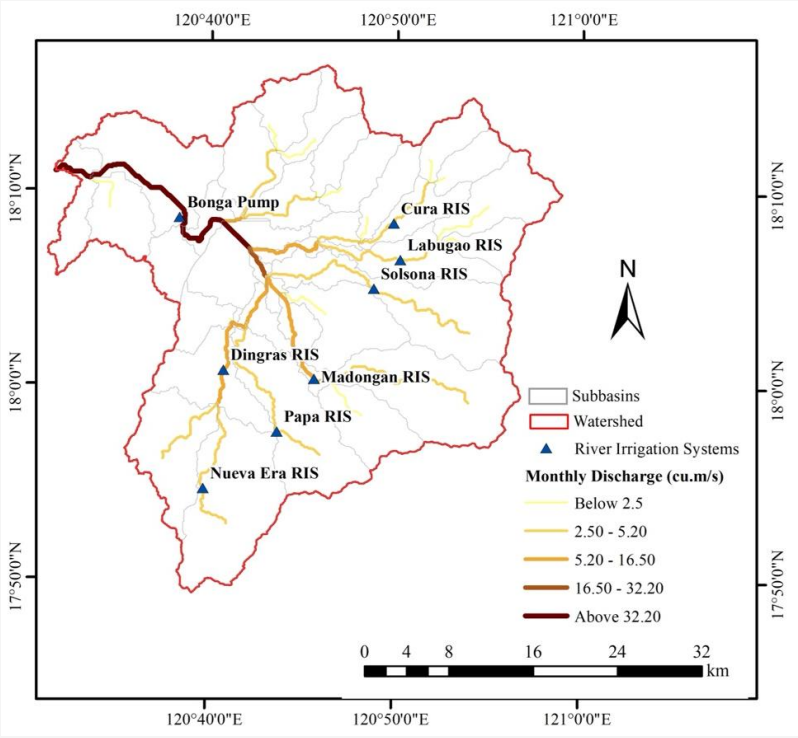

Figure 4: Location of the eight River Irrigation Systems (RIS) in the Padsan River watershed, showing monthly discharge categories (2003–2021)

3.3 Seasonal Variations and Spatial Disparities of River Discharge

The SWAT-simulated monthly river discharge data demonstrate significant spatiotemporal heterogeneity across the eight major River Irrigation Systems (RIS) in the PRW (Figure 4). The spatial component, as shown in Figure 4, highlights how water resources are unevenly distributed across the RIS along with the river networks. Bonga Pump stations sustain most of the water flow (>32 m^3/s monthly flow), accounting for potential surface water availability. At the same time, smaller systems, such as Labugao, Cura, Solsona, and Nueva Era, rarely exceed 10 m^3, exposing them to recurring water stress. Mid-range systems, such as Madongan, Dingras, and Papa, occupy intermediate categories. (16-32 m^3/s), reflecting moderate but seasonally variable flows.

The seasonal component (Figure 5) underscores the strong influence of the Type 1 climate. All RIS experience peak flows during September-October, aligned with the southwest monsoon and typhoon season, and minimum flows during April-May, when rainfall is sparse. Dingras RIS demonstrates the most pronounced fluctuation, with wet-season discharges nearly 3.4 times higher than dry-season values. At the same time, Bonga Pump sustains consistently higher flows, underscoring its role as the most reliable year-round source of surface water. By contrast, smaller RIS such as Labugao and Nueva Era remain consistently low, reinforcing their vulnerability to droughts and dry-season deficits.

These seasonal variations and spatial disparities have direct implications for governance. The dominance of Bonga Pump highlights the potential for a redistributed allocation and diverse infrastructure to balance flows across the watershed, with lower water availability and those with higher potential for water availability. Wet-season surpluses in Madongan and Papa RIS (16-23 m^3/s) present opportunities for Managed Aquifer Recharge (MAR), ensuring that surplus water can be stored for use in the dry season and potentially reduce overflow that contributes to flash floods. Persistently low-flow systems, such as Labugao and Nueva Era, require tight groundwater abstraction regulation and conjunctive use strategies to avoid aquifer depletion. The identification of high-discharge zones also suggests potential sites for new RIS or surface water diversion projects, reducing the over-reliance on groundwater extraction. Together, these findings establish a spatiotemporal hydrological baseline that supports equitable water allocation, MAR prioritization, irrigation scheduling, conjunctive use allocation management, and climate-resilient governance in the watershed.

3.4 Spatial Variability of Groundwater Recharge and Associated LULC and Population Distribution

In PRW, the total agricultural area is 393.10 km², while the total RIS service area is only 75.77 km² [13], which accounts for 19.27% of the total productive area. For this reason, farmers heavily relied on the communal river irrigation system and groundwater extraction during the dry season [28]. This reliance elevates the strategic importance of groundwater recharge, particularly in light of increasing hydroclimatic variability and water demand. The SWAT-simulated seasonal groundwater recharge map (Figure 6) reveals that the recharge potential varies widely across the watershed, with the highest recharge of 700 mm/year concentrated in the forested uplands of the southern and southeastern PRW.

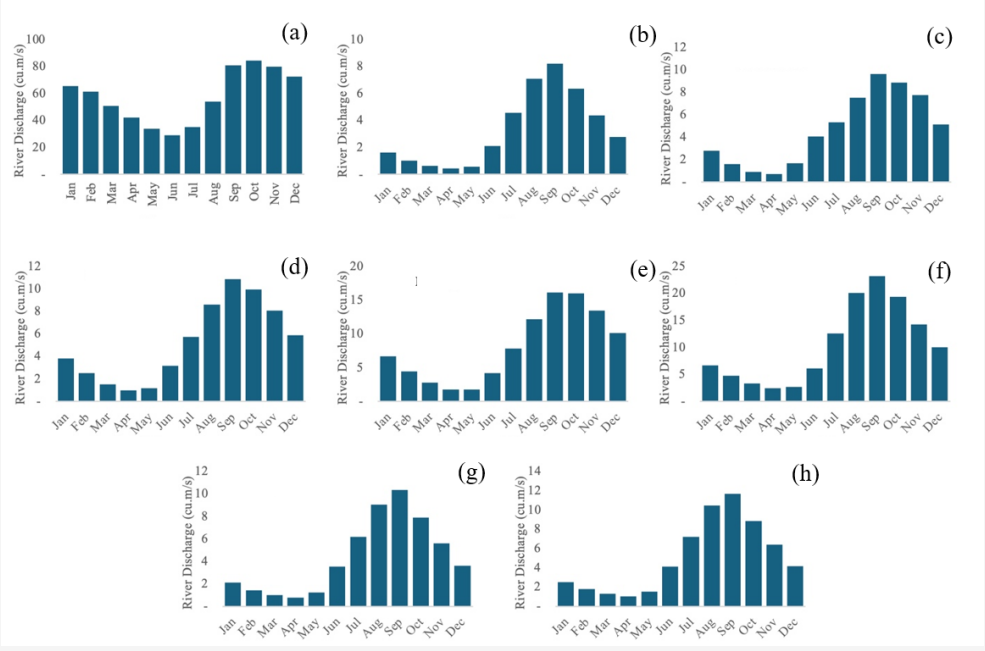

Figure 5: SWAT-simulated monthly river discharge from 2003 to 2021 for each of the eight RIS in the Padsan River watershed (a) Bonga pump, (b) Cura, (c) Solsona, (d) Labugao, (e) Madongan, (f) Dingras, (g) Papa, and (h) Nueva Era

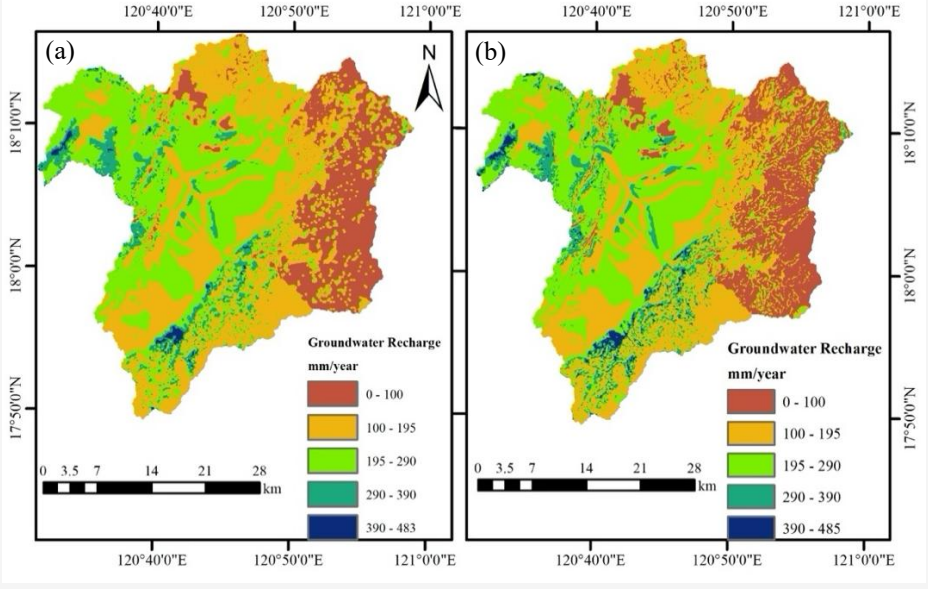

Figure 6: Spatial distribution of groundwater recharge (a) the wet season, and (b) the dry season

3.4 Spatial Variability of Groundwater Recharge and Associated LULC and Population Distribution

In PRW, the total agricultural area is 393.10 km², while the total RIS service area is only 75.77 km² [13], which accounts for 19.27% of the total productive area. For this reason, farmers heavily relied on the communal river irrigation system and groundwater extraction during the dry season [28]. This reliance elevates the strategic importance of groundwater recharge, particularly in light of increasing hydroclimatic variability and water demand. The SWAT-simulated seasonal groundwater recharge map (Figure 6) reveals that the recharge potential varies widely across the watershed, with the highest recharge of 700 mm/year concentrated in the forested uplands of the southern and southeastern PRW. Conversely, the lower recharge zones, often located in intensive agricultural areas, exhibit recharge rates of around 300 mm/year.

Furthermore, the illustration of seasonal groundwater recharge (Figure 6) in the watershed reveals an unexpected pattern: the total recharge during the dry season is almost equal to that of the wet seasons in most sub-basins. Wet-season recharge groundwater up to 483 mm/year, while during the dry season, it can recharge up to 485 mm/year. This apparent anomaly reflects the delayed downward movement of recharge water through the unsaturated zone (vadose zone), where rainfall infiltrated during the wet season is temporarily stored in the soil and deeper unsaturated layers before gradually percolating downward to the water table. As a result, aquifer replenishment continues even after rainfall has diminished, with recharge peaks occurring during the subsequent dry months. This finding highlights the buffering function of the unsaturated zone in sustaining groundwater supply across seasons. From a governance perspective, protecting areas with high infiltration capacity, particularly lowland and valley-bottom zones, becomes critical, as land degradation or surface sealing could significantly reduce this delayed recharge mechanism and compromise dry-season water availability.

The spatial variability of groundwater recharge reflects underlying LULC patterns (Table 5, Figure 7). Pasture and range-brush areas exhibit the highest recharge rates (568 mm and 478 mm), consistent with their permeable grass-shrub cover. This is followed by forests (420-440 mm), which are critical for sustaining baseflow and aquifer recharge. In contrast, agricultural lands, despite their large spatial footprint and the most considerable demand for irrigation, yield a lower mean recharge of only 365.95 mm, suggesting limitations due to surface runoff, compaction, and reduced infiltration capacity, despite their lower slopes, which may be potentially prone to flash flooding.

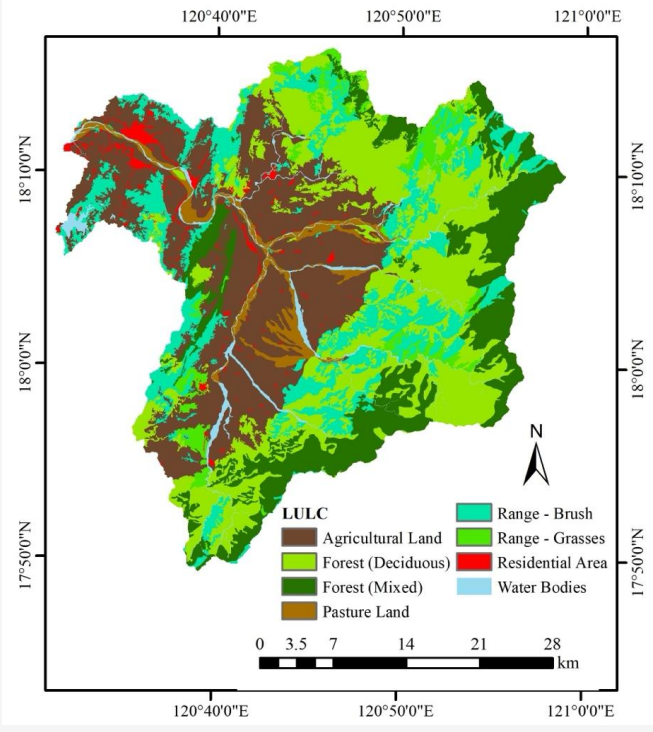

Figure 7: PRW LULC

Table 5: Annual groundwater recharge at different LULC

LULC	Description Copernicus (CLC) Nomenclature [48]	Area, km² (%)	Annual Groundwater Recharge, (mm)
Pasture	Grassland managed or used for grazing and forage production (CLC 231)	43.55 (3.28)	585.99
Range Brush	Shrub and/or herbaceous vegetation associations, with open shrub cover often mixed with grasses. (CLC 322)	219.64 (16.57)	478.28
Forest (Mixed)	Mixed stands of broad-leaved and coniferous tress with no single type dominating (CLC 313)	211.22 (15.93)	441.02
Forest (Deciduous)	Broad-leaved forest where tree species shed foliage seasonality (CLC 311)	377.80 (28.50)	420.33
Residential Areas	Urban fabric including continuous or discontinuous built-up areas (CLC 111-112)	23.57 (1.78)	389.71
Agricultural Land	Areas under cultivation including arable fields, permanent crops, and mixed agricultural mosaics (CLC 211-244)	393.10 (29.65)	365.95
Range Grasses	Natural or semi-natural grasslands with little or no woody vegetation.	56.94 (4.29)	312.9
	Total	1,325.82 (100)	Average = 427.18

Table 6: Hydrogeological attributes and its population percentage in the PR

Groundwater Systems	Map Legend Description (Class)	Area (%)	Pop. den. (pop. /km²) total (%)	Recharge (mm/year)
Rocks in which flows are dominantly intergranular				
Extensive and highly productive aquifers	Extensive and highly productive (Class 1)	30.02	78.00	394.98
Fairly extensive and productive aquifers	Fairly extensive and productive (Class 2)	6.81	9.25	445.11
Local and less productive aquifers	Local and less productive (Class 3)	16.29	11.18	385.11
Rocks in which flow is dominantly through fractures and/or solution openings				
Fairly extensive and productive aquifers with highly potential recharge	Fairly extensive and productive (Class 2)	24.27	1.20	302.96
Fairly to less extensive and productive aquifers with low to moderate potential recharge	Fairly to less extensive and productive (Class 3)	0.44	-	294.59
Local groundwater—regions underlain by impermeable rocks generally without significant groundwater except in residuum, sufficiently leached and/or fractured zone				
Rocks with limited potential, low to moderate permeability	Limited potential (Class 4)	21.08	0.36	291.59
Rocks without any known significant groundwater obtained through drilled wells. Largely untested	No significant groundwater (Class 4)	0.08	0.01	430.30

While current recharge hotspots occur in pasture, range-brush, and forestlands, conversion of these areas into cropland or settlements could significantly reduce infiltration and groundwater replenishment. Similarly, projected increases in rainfall intensity and extended dry periods under climate change may alter seasonal recharge dynamics, limiting infiltration during wet months and reducing baseflow in dry months. These potential shifts highlight the need to consider land use trajectories and climate futures in groundwater governance to safeguard recharge zones and maintain aquifer sustainability. Hydrogeological classification (Table 6) further contextualizes this spatial variability. Approximately 30% of the watershed is underlain by an extensive and highly productive intergranular aquifer, which not only provides significant storage but also supports 78% of the total population, indicating a strong convergence of demand and aquifer productivity.

However, 21.08% of the area lies in zones with limited potential, making sustainable recharge and abstraction management essential for long-term viability.

The spatial heterogeneity of groundwater recharge and aquifer productivity in PRW assumes greater significance when viewed in conjunction with LULC and population distribution. Recharge hotspots occur in pasture, range brush, and forestlands; yet, these areas are increasingly vulnerable to land-use change, which may diminish infiltration and storage capacity. At the same time, agricultural zones, despite their extensive footprint and irrigation demand, exhibit comparatively lower recharge, underscoring a potential mismatch between water availability and demand. Hydrogeological classification further reveals that highly productive aquifers coincide with 78% of the population, intensifying pressure on the productive groundwater systems. These patterns highlight the governance challenge of protecting recharge zones, regulating abstraction where population pressure is most significant, and anticipating the compounded risks of urban expansion and climate extremes, which could further shift recharge dynamics.

The necessity of identifying and protecting recharge zones, particularly in areas where productive aquifers intersect with high-demand zones but face declining recharge due to land-use change or excessive pumping. Moreover, groundwater governance strategies such as Managed Aquifer Recharge should prioritize high-recharge zones (e.g., pasture and forestlands) while enforcing strict abstraction in vulnerable areas with limited potential.

3.5 Data-driven Geospatial Governance Insights

The integrated SWAT, remote sensing, and hydrogeological analysis for PRW reveals evident spatial inequities in water access and crucial opportunities for sustainable governance. Current RIS contributes about one-fourth of the agricultural landscape, compelling farmers, particularly those outside service areas, to rely heavily on groundwater extraction [49] and unmanaged river flow pumping. These practices strain aquifer and river systems, especially during dry periods, and underscore the crucial role of groundwater recharge in sustaining livelihoods and ensuring water security. The monthly discharge estimated by the hydrological model enables the potential expansion of RIS, capturing the benefits of surface flow and promoting conjunctive governance. The spatial heterogeneity of the simulated discharge at different rivers is presented in Figure 4, which contributes to the feasibility assessment of RIS infrastructure expansion to increase productivity in underserved agricultural zones. These expansions should prioritize adaptation to climate variability and the inclusivity of farmers' needs. The increasing climate variability, as supported by the growing model bias during the validation period, suggests that irrigation infrastructure, both existing and future initiatives, must carefully account for the climate variability that significantly affects river discharge patterns. Furthermore, by aligning new RIS development with high-discharge zones (Figure 4), especially in the lower stream alongside high population density, planners can support equitable surface water distribution and reduced groundwater reliance. This is in response to the fact that the productive aquifer in the area supports 78% of the population; thus, conjunctive use governance and management are highly recommended.

Furthermore, the high flow yield of the existing Bonga Pump could contribute to the feasibility of MAR in the area, which would assist not only in providing irrigation but also support industrial use, residential use, and the expansion of irrigation services. Meanwhile, other RIS with lower discharge flow, (e.g., Cura RIS, Labugao RIS, Papa RIS, and Solsona RIS) can implement proper conjunctive use management and governance of water resources to ensure sustainability of both surface and subsurface water resources.

On the other hand, seasonal maps show that dry-season recharge is nearly equal to wet-season totals due to lagged downward movement of water in the unsaturated zone. Recognizing this buffering role of delayed recharge in water allocation planning could lead to strategic multi-season recharge dynamics in future water infrastructure initiatives, such as MAR structure design considerations. Subsequently, percolated water that remained in the unsaturated zone maintained soil moisture, as shown by seasonal groundwater recharge. The continuous urbanization triggered by socio-economic development could disrupt these dynamics and contribute to land subsidence; hence, groundwater recharge assessment is very important for city planning. MAR technologies have been validated globally as both feasible and efficient [50][51][52][53] and [54]. A notable example is the MAR via Soil Aquifer Treatment (SAT) basins in Israel, where it is internationally recognized as one of the most successful aquifer recharge schemes [55].

Agricultural lands cover the most significant area but yield low recharge compared to other LULC classes, indicating a high potential mismatch between demand and supply. For this notion, the study recommends enhancing efficiency through modernized systems and water-saving practices (e.g.,

drip or deficit irrigation) to reduce stress on groundwater. Agricultural land areas are primarily located in lower to midstream (Figure 6), where slopes are flat to gentle (Figure 1). These locations can serve as suitable sites for Agricultural MAR (AgMAR) that can serve as water harvesting for both rainfall and runoff during the rainy season, which can provide irrigation during the dry season without over-extracting from groundwater. According to the evaluation conducted on AgMAR in Vietnam [56], it can be operated by farmers and is a promising approach for climate change adaptation. Furthermore, the spatial and temporal heterogeneity of river discharge and the seasonal groundwater recharge can significantly contribute to achieving climate-smart agriculture through comprehensive cropping calendar adjustments and efficient irrigation schedules.

In contrast, strict groundwater abstraction limits are necessary in low-discharge areas like Nueva Era and Labugao RIS, which are identified to have lower flow according to the study's findings. These regions require conjunctive-use frameworks that balance abstraction with periodic recharge, a long-standing water management strategy, to halt overdraft and preserve aquifer integrity [50][57] and [58].

While the SWAT-simulated recharge and discharge patterns provide valuable spatial insights, these outputs are subject to several uncertainties that extend beyond calibration statistics. The use of bias-corrected satellite rainfall (CHIRPS) and ERA5 temperature data introduces potential biases from coarse resolution and imperfect correction of local rainfall extremes, particularly during typhoons. Similarly, population distribution was inferred from Google-derived building datasets, which approximate settlement density but may not fully capture demographic heterogeneity, especially in highly dense areas in the watershed where large and commercial buildings are not occupied. Hydrogeological units were based on national-scale MGB maps (1:125,000), which provide broad aquifer classifications but cannot resolve finer-scale variability in the aquifer. Despite these limitations, the integrated patterns, such as the concentration of recharge in pasture and forestlands, the potential mismatch between irrigation demand and recharge in agricultural zones, and the convergence of 78% of the population on a highly productive aquifer, are consistent across datasets and valuable insights for governance interventions. These findings, though not absolute, are sufficiently robust to inform governance strategies that prioritize recharge zone protection, regulate abstraction in high-demand aquifer units, and integrate spatial variability into land and water resources planning.

Lastly, a central pillar of this governance-integrated model is the establishment of a GIS-based and data-driven decision support system that integrates hydrological outputs, recharge maps, hydrogeological attributes, land use, infrastructure, and demographic layers. Such a tool would empower watershed managers and stakeholders to monitor recharge and discharge in real-time, prioritize RIS expansion and MAR sites, regulate abstraction, and evaluate adaptive strategies, a transformative step toward data-driven, equitable, and climate-resilient water resource management.

4. Conclusions

This study presents a data-driven, geospatial governance framework for PRW by explicitly linking hydrological simulations with recharge mapping, LULC patterns, and population overlays. Beyond characterizing recharge heterogeneity, the study's scientific contributions lie in demonstrating how seasonal recharge dynamics and aquifer-population convergence, with the novel use of Google Building Footprints, can be operationalized into governance strategies such as MAR potential zones, abstraction regulation, climate-smart irrigation, and the implementation of conjunctive use management and governance. This integration advances the application of SWAT from hydrological modeling toward decision support for groundwater governance in Philippine watersheds, providing a transferable approach for data-scarce basins in the tropics, with the potential assessment of socio-economic development in the context of water resources through fine-resolution population estimates. Nonetheless, several limitations should be addressed in this state-of-the-art approach, including the reliance on bias-corrected satellite rainfall and reanalysis temperature datasets, which introduce input uncertainty; the use of Google building footprint-based population estimates and coarse institutional datasets and maps constrain model performance and demographic and aquifer precision. Future research should address these limitations by integrating future higher-resolution hydrogeological and geological surveys and socio-economic datasets beyond population spatial distribution. Future research may explore the impacts of climate and LULC change on water resources, as well as the effects of the expansion and spatial pattern of migration in the watershed on water resources.

Furthermore, field-based validation of MAR feasibility in identified recharge hotspots would further strengthen the operational applicability of these findings. By recognizing these limitations while underscoring the value of geospatial integration, this study highlights a pathway toward climate-resilient and evidence-based groundwater governance in the Philippines.

References

[1] Gleeson, T., Wada, Y., Bierkens, M. F. P. and van Beek, L. P. H., (2012). Water Balance of Global Aquifers Revealed by Groundwater Footprint. *Nature*, Vol. 488(7410), 197–200. https://doi.org/10.1038/nature11295.

[2] Taylor, R. G., Scanlon, B. R., Döll, P., Rodell, M., van Beek, L. P. H., Wada, Y., Longuevergne, L., Leblanc, M., Famiglietti, J. S., Edmunds, M., Konikow, L. F., Green, T. R., Chen, J., Taniguchi, M., Bierkens, M. F. P., MacDonald, A., Fan, Y., Maxwell, R. M., Yechieli, Y., Gurdak, J. J., Allen, D. M., Shamsudduha, M., Hiscock, K., Yeh, P. J. F., Holman, I. and Treidel, H., (2012). Groundwater and Climate Change. *Nature Climate Change*, Vol. 3(4), 322–329. https://doi.org/10.1038/NCLIMATE1744.

[3] Kundzewicz, Z. W., Mata, L. J., Arnell, N. W., Doll, P., Jimenez, B., Miller, K., Oki, T., Sen, Z. and Shiklomanov, I. A., (2008). The Implications of Projected Climate Change for Freshwater Resources and their Management. *Hydrological Sciences Journal*, Vol. 53(1), 3–10. https://doi.org/10.1623/hysj.53.1.3.

[4] Stigter, T. Y., Miller, J., Chen, J. and Re, V., (2023). Groundwater and Climate Change: Threats and Opportunities. *Hydrogeology Journal*, Vol. 31(1), 7–10. https://doi.org/10.1007/s10040-022-02554-w.

[5] Rola, A. C., Pulhin, J. M., Tabios, G. Q., Lizada, J. C. and Dayo, M. H. F., (2015). Challenges of Water Governance in the Philippines. *Philippine Journal of Science*, Vol. 144(2), 197–208. https://doi.org/10.21142/pjs.144.02.15.

[6] Valenzuela, E. D. and Gutierrez, E. C., (2019). CPBRD Policy Brief: Addressing Institutional Challenges in Water Resources Management. Congressional Policy and Budget Research Department. [Online]. Available: https://cpbrd.congress.gov.ph/images/PDF%20Attachments/CPBRD%20Policy%20Brief/PB2019-01_Addressing_Institutional_Challenges.pdf [Accessed: Nov. 5, 2024].

[7] Provincial Government of Ilocos Norte. (2021). *2022 Ecological Profile Province of Ilocos Norte*. Provincial Planning and Development Office.

[8] Tolentino, P. L. M., Cinco, T. A., Hilario, F. D., De Guzman, R. G., Ortega, D. V., Narisma, G. T. and Gutierrez, A., (2016). Projected Impact of Climate Change on Hydrological Regimes in the Philippines. *PLOS ONE*, Vol. 11(10). https://doi.org/10.1371/journal.pone.0163941.

[9] Lazaro, F., (2024). Ilocos Norte Sustains ₱38.26 M in Damage to Agriculture from El Niño. Manila Bulletin. [Online]. Available: https://mb.com.ph/2024/5/16/ilocos-norte-sustains-p38-26-m-in-damage-to-agriculture-from-el-nino-1 [Accessed: Dec. 29, 2024].

[10] Abbaspour, K. C., Vaghefi, S. and Srinivasan, R., (2017). A Guideline for Successful Calibration and Uncertainty Analysis for Soil and Water Assessment: A Review of Papers from the 2016 International SWAT Conference. *Water*, Vol. 10(1). https://doi.org/10.3390/w10010006.

[11] Arnold, J. G., Moriasi, D. N., Gassman, P. W., Abbaspour, K. C., White, M. J., Srinivasan, R., Santhi, C., Harmel, R. D., Van Griensven, A., Van Liew, M. W., Kannan, N. and Jha, M. K., (2012). SWAT: Model Use, Calibration, and Validation. *Transactions of the ASABE*, Vol. 55(4), 1491–1508. https://doi.org/10.13031/2013.42256.

[12] Guiamel, I. A. and Lee, H. S., (2020). Potential Hydropower Estimation for the Mindanao River Basin in the Philippines Based on Watershed Modelling Using the Soil and Water Assessment Tool. *Energy Reports*, Vol. 6, 1010–1028. https://doi.org/10.1016/j.egyr.2020.04.025.

[13] Jimenez, J. I., Tripathi, N. K., Pandey, A., Chao, K. C. and Shrestha, S., (2025). Assessment of the Spatiotemporal Dynamics of River Discharge and Groundwater Recharge to Support Sustainable Water Management for Irrigated Agriculture in the Padsan River Watershed. *Earth Science Informatics*, Vol. 18(2), 1–21. https://doi.org/10.1007/s12145-025-01707-1.

[14] Jimenez, J. I., Alibuyog, N., Manzano, V. J., Calixto, B. G., Caoili, R. and Pascual, C., (2022). Quantifying Impacts of Climate and Land Use Change on Groundwater Hydrology and Sustainability of the Quaioit River Watershed. In *Proceedings of the 2nd International Conference on Education and Technology (ICETECH 2021)*, Vol. 63, 102–

108. https://doi.org/10.2991/assehr.k.220103.018.

[15] Boongaling, C. G. K., Faustino-Eslava, D. V. and Lansigan, F. P., (2018). Modeling Land Use Change Impacts on Hydrology and the Use of Landscape Metrics as Tools for Watershed Management: The Case of an Ungauged Catchment in the Philippines. *Land Use Policy*, Vol. 72, 116–128. https://doi.org/10.1016/j.landusepol.2017.12.042.

[16] Sirko, W., Kashubin, S., Ritter, M., Annkah, A., Bouchareb, Y. S. E., Dauphin, Y., Keysers, D., Neumann, M., Cissé, M. and Quinn, J., (2021). Continental-Scale Building Detection from High-Resolution Satellite Imagery. arXiv:2107.12283. [Online]. Available: https://arxiv.org/abs/2107.12283 [Accessed: Sep. 22, 2025].

[17] Tambong, A., Bacordo, L., Martinez, K. Y., Molato, L. A., Semblante, O. and Garcia, P., (2019). Hydropower Potentials Estimation of Biliran Islands Based on Synthetic Aperture Radar Spatial Data Using Soil and Water Assessment Tool Simulation. *Science and Humanities Journal*, Vol. 13(1), 83–98. https://doi.org/10.47773/SHJ.1998.121.7.

[18] Tiongson, R. M. T. and Bolanio, K. P., (2020). Modeling and Estimation of Run-of-River Hydropower Potential Through Integrated GIS and SWAT Interface in Agusan River Basin. *TENCON 2020 – IEEE Region 10 Conference*, 527–531. https://doi.org/10.1109/TENCON50793.2020.9293936.

[19] Uy, H. C., Quebada, A. E. E. and Amante, M. L. P., (2023). Hydropower Generation Potential of Samar River System Based on GIS and SWAT Model. *GMSARN International Journal*, Vol. 17(1), 33–39. [Online]. Available: https://gmsarnjournal.com/home/wp-content/uploads/2022/05/vol17no1-5.pdf [Accessed: Sep. 23, 2025].

[20] Alejo, L. A., Ella, V. B., Lampayan, R. M. and Delos Reyes, A. A., (2021). Assessing the Impacts of Climate Change on Irrigation Diversion Water Requirement in the Philippines. *Climatic Change*, Vol. 165(3–4), 1–15. https://doi.org/10.1007/s10584-021-03080-6.

[21] Abbas, S. A., Xuan, Y. and Bailey, R. T., (2022). Assessing Climate Change Impact on Water Resources in Water Demand Scenarios Using SWAT-MODFLOW-WEAP.*Hydrology*, Vol. 9(10). https://doi.org/10.3390/hydrology9100164.

[22] Alshammari, E., Abdul Rahman, A., Ranis, R., Abu Seri, N., and Ahmad, F. (2024). Investigation of Runoff and Flooding in Urban Areas based on Hydrology Models: A Literature Review. *International Journal of Geoinformatics*, Vol. 20(1); 99–119. https://doi.org/10.52939/ijg.v20i1.3033.

[23] Barthel, R. and Banzhaf, S., (2016). Groundwater and Surface Water Interaction at the Regional-Scale – A Review with Focus on Regional Integrated Models. *Water Resources Management*, Vol. 30(1), 1–32. https://doi.org/10.1007/s11269-015-1163-z.

[24] Along, A., Orboc, D. R. and Calagui, L., (2024). Floristic Inventory, Diversity, and Community Structure of the Riparian and Coastal Sand Dune Landscapes in the Lower Padsan River Basin, Laoag City, Ilocos Norte, Philippines. *Journal of Ecosystem Science and Eco-Governance*, Vol. 6(1), 20–33. https://doi.org/10.54610/jeseg.v6i1.85.

[25] Philippine Atmospheric, Geophysical and Astronomical Services Administration-Department of Science and Technology [PAGASA-DOST]. (2025). Climate Map of the Philippines (1951–2010) [Map]. Climatology and Agrometeorology Division, Philippine Atmospheric, Geophysical and Astronomical Services Administration. [Online Map]. Available: https://www.pagasa.dost.gov.ph/information/climate-philippines [Accessed: May 28, 2025].

[26] Corporal-Lodangco, I. L. and Leslie, L. M., (2017). Defining Philippine Climate Zones Using Surface and High-Resolution Satellite Data. *Procedia Computer Science*, Vol. 114, 324–332. https://doi.org/10.1016/j.procs.2017.09.068.

[27] Intergovernmental Panel on Climate Change [IPCC]. (2023). Climate Change 2023: Synthesis Report. Contribution of Working Groups I, II and III to the Sixth Assessment Report of the Intergovernmental Panel on Climate Change (H. Lee and J. Romero, Eds.). IPCC, Geneva, Switzerland, 35–115. https://doi.org/10.59327/IPCC/AR6-9789291691647.

[28] Alonzo, C. A., Galabay, J. M., Macatangay, M. N., Magpayo, M. B. and Ramirez, R., (2023). Drought Risk Assessment and Monitoring of Ilocos Norte Province in the Philippines Using Satellite Remote Sensing and Meteorological Data. *AgriEngineering*, Vol. 5(2), 720–739. https://doi.org/10.3390/agriengineering5020045.

[29] Khalid, K., Ali, M. F., Abd Rahman, N. F. A., Mispan, M. R., Haron, S. H., Othman, Z. and Bachok, M. F., (2016). Sensitivity Analysis in Watershed Model Using SUFI-2 Algorithm. *Procedia Engineering*, Vol. 162, 441–447. https://doi.org/10.1016/j.proeng.2016.11.086.

[30] Enayati, M., Bozorg-Haddad, O., Bazrafshan, J., Hejabi, S. and Chu, X., (2021). Bias Correction Capabilities of Quantile Mapping Methods for Rainfall and Temperature Variables. *Journal of Water and Climate Change,* Vol. 12(2), 401–419. https://doi.org/10.2166/wcc.2020.261.

[31] Themeßl, M. J., Gobiet, A. and Leuprecht, A., (2011). Empirical-Statistical Downscaling and Error Correction of Daily Precipitation from Regional Climate Models. *International Journal of Climatology*, Vol. 31(10), 1530–1544. https://doi.org/10.1002/joc.2168.

[32] Gudmundsson, L., Bremnes, J. B., Haugen, J. E. and Engen-Skaugen, T., (2012). Technical Note: Downscaling RCM Precipitation to the Station Scale Using Statistical Transformations – A Comparison of Methods. *Hydrology and Earth System Sciences*, Vol. 16(9), 3383–3390. https://doi.org/10.5194/hess-16-3383-2012.

[33] Cannon, A. J., Sobie, S. R. and Murdock, T. Q., (2015). Bias Correction of GCM Precipitation by Quantile Mapping: How Well Do Methods Preserve Changes in Quantiles and Extremes?. *Journal of Climate*, Vol. 28(17), 6938–6959. https://doi.org/10.1175/JCLI-D-14-00754.1.

[34] Moriasi, D. N., Gitau, M. W., Pai, N. and Daggupati, P., (2015). Hydrologic and Water Quality Models: Performance Measures and Evaluation Criteria. *Transactions of the ASABE*, Vol. 58(6), 1763–1785. https://doi.org/10.13031/trans.58.10715.

[35] Anaba, L. A., Banadda, N., Kiggundu, N., Wanyama, J., Engel, B. and Moriasi, D., (2017). Application of SWAT to Assess the Effects of Land Use Change in the Murchison Bay Catchment in Uganda. *Computational Water, Energy, and Environmental Engineering*, Vol. 6(1), 24–40. https://doi.org/10.4236/cweee.2017.61003.

[36] Neitsch, S. L., Arnold, J. G., Kiniry, J. R., Williams, J. R. and King, K. W., (2002). Soil and Water Assessment Tool – Theoretical Documentation: Version 2000. Texas Water Resources Institute Report TR-191; Grassland, Soil & Water Research Laboratory, Agricultural Research Service, Temple, Texas; Blackland Research Center, Texas Agricultural Experiment Station, Texas.1-808.

[37] Abbaspour, K. C., (2015). SWAT-CUP: SWAT Calibration and Uncertainty Programs – User Manual. Texas A&M AgriLife/Eawag. [Online]. Available: https://swat.tamu.edu/media/114860/usermanual_swatcup.pdf [Accessed: Jan. 31, 2024].

[38] Mines and Geosciences Bureau. (2024). Hydrogeologic Map of the Province of Ilocos Norte. [Online]. Available: https://controlmap.mgb.gov.ph/portal/apps/instant/attachmentviewer/index.html?appid=3ce7883788d04f8e997686fe677b2efc [Accessed: Sep. 13, 2025].

[39] Department of Environment and Natural Resources. (2024). DENR Annual Report for FY 2022. [Online]. Available: https://denr.gov.ph/wp-content/uploads/2024/04/DENR-Annual-Report-for-FY2022_.pdf [Accessed: Sep. 13, 2025].

[40] Hodson, T. O., (2022). Root-Mean-Square Error (RMSE) or Mean Absolute Error (MAE): When to Use Them or Not. *Geoscientific Model Development*, Vol. 15(14), 5481–5487. https://doi.org/10.5194/gmd-15-5481-2022.

[41] Trentini, L., Dal Gesso, S., Venturini, M., Guerrini, F., Calmanti, S. and Petitta, M., (2023). A Novel Bias Correction Method for Extreme Events. *Climate*, Vol. 11(1). https://doi.org/10.3390/cli11010003.

[42] Omondi, C. K., Rientjes, T. H. M., Booij, M. J. and Nelson, A. D., (2024). Satellite Rainfall Bias Correction Incorporating Effects on Simulated Crop Water Requirements. *International Journal of Remote Sensing*, Vol. 45(7), 2269–2288. https://doi.org/10.1080/01431161.2024.2326801.

[43] Kulsoontornrat, J., and Puangkaew, N. (2025). Assessing the Impacts of Land Use and Land Cover Changes on Sediment Yield Using the SWAT Model: A Case Study in the Khlong Bang Yai Watershed, Phuket Island, Thailand. *International Journal of Geoinformatics*, Vol. 21(5); 62–79. https://doi.org/10.52939/ijg.v21i5.4161

[44] Marin, M., Mihailescu, D., Birsan, M. V. and Cheval, S., (2020). Assessing the Vulnerability of Water Resources in the Context of Climate Changes in a Small Forested Watershed Using SWAT: A Review. *Environmental Research*, Vol. 184. https://doi.org/10.1016/j.envres.2020.109330.

[45] Guiamel, I. A. and Lee, H. S., (2020). Watershed Modelling of the Mindanao River Basin in the Philippines Using the SWAT for Water Resource Management. *Civil Engineering Journal (Iran)*, Vol. 6(4), 626–648. https://doi.org/10.28991/cej-2020-03091496.

[46] Hong, J., Agustin, W., Yoon, S. and Park, J. S., (2022). Changes of Extreme Precipitation in the Philippines, Projected from the CMIP6 Multi-Model Ensemble. *Weather and Climate Extremes*, Vol. 37. https://doi.org/10.1016/j.wace.2022.100480.

[47] Department of Science and Technology. (2016). DOST 2016 Annual Report: A Modernized PAGASA Equipped with Advanced Technology and a Global Competitive Workforce. [Online]. Available: https://pubfiles.pagasa.dost.gov.ph/pagasaweb/files/hmd/tramsparency/2016_Annual_Report.pdf [Accessed: Sep. 16, 2025].

[48] Feranec, J., Jaffrain, G., Soukup, T. and Hazeu, G., (2010). Determining Changes and Flows in European Landscapes 1990–2000 Using CORINE Land Cover Data. *Applied Geography*, Vol. 30(1), 19–35. https://doi.org/10.1016/j.apgeog.2009.07.003.

[49] Alonzo, C. A., Galabay, J. M., Macatangay, M. N., Magpayo, M. B. and Ramirez, R., (2023). Drought Risk Assessment and Monitoring of Ilocos Norte Province in the Philippines Using Satellite Remote Sensing and Meteorological Data. *AgriEngineering*, Vol. 5(2), 720–739. https://doi.org/10.3390/agriengineering5020045.

[50] Yosef, Z.-M., Birhanu, B., Suryabhagavan, K. V. and Tsegay, T., (2024). GIS-Based Suitability Mapping of Managed Aquifer Recharge (MAR) in Diredawa Catchment, Eastern Ethiopia. *International Journal of River Basin Management*, 1–15. https://doi.org/10.1080/15715124.2024.2361038.

[51] Salameh, E., Abdallat, G, and van der Valk, M., (2019). Planning Considerations of Managed Aquifer Recharge (MAR) Projects in Jordan. *Water*, Vol. 11(2). https://doi.org/10.3390/w11020182.

[52] Morrisett, C. N., Van Kirk, R. W. and Null, S. E., (2024). Can Agricultural Managed Aquifer Recharge (Ag-MAR) Recover Return Flows Under Prior Appropriation in a Warming Climate? *Water Resources Research*, Vol. 60(8). https://doi.org/10.1029/2023WR036648.

[53] Sufyan, M., Martelli, G., Teatini, P., Cherubini, C., and Goi, D. (2024). Managed Aquifer Recharge for Sustainable Groundwater Management: New Developments, Challenges, and Future Prospects. *Water*, Vol. 16(22). https://doi.org/10.3390/w16223216.

[54] Itani, N., Harik, G., Alameddine, I. and El-Fadel, M., (2022). Managed Aquifer Recharge in Karstic Systems: Site Suitability Mapping by Coupling Multi-Criteria Decision Analysis with Remote Sensing and Hydrologic Modeling. *Journal of Environmental Management*, Vol. 322. https://doi.org/10.1016/j.jenvman.2022.116162.

[55] Elkayam, R. and Lev, O., (2024). Head-Independent Infiltration Rate in Aquifer Recharge with Treated Municipal Wastewater. *ACS ES&T Water*, Vol. 4(12), 5678–5688. https://doi.org/10.1021/acsestwater.4c00668.

[56] Pavelic, P., Dinh, N. V., Pham, Q. T., Tran, N. T. and Cordery, I., (2022). Evaluation of Managed Aquifer Recharge in the Central Highlands of Vietnam. *Journal of Hydrology: Regional Studies*, Vol. 44. https://doi.org/10.1016/j.ejrh.2022.101257.

[57] Kourakos, G., Dahlke, H. E. and Harter, T., (2019). Increasing Groundwater Availability and Seasonal Base Flow Through Agricultural Managed Aquifer Recharge in an Irrigated Basin. *Water Resources Research*, Vol. 55(9). 7464–7492. https://doi.org/10.1029/2018WR024019.

[58] Aloui, S., Zghibi, A., Mazzoni, A., Elomri, A. and Al-Ansari, T., (2024). Identifying Suitable Zones for Integrated Aquifer Recharge and Flood Control in Arid Qatar Using GIS-Based Multi-Criteria Decision-Making. *Groundwater for Sustainable Development*, Vol. 25. https://doi.org/10.1016/j.gsd.2024.101137.